

# Electrochemical Stability and Degradation of Commercial Pd/C Catalyst in Acidic Media

Milutin Smiljanić,\* Marjan Bele, Leonard Moriau, Francisco Ruiz-Zepeda, Martin Šala, and Nejc Hodnik\*

Cite This: *J. Phys. Chem. C* 2021, 125, 27534–27542

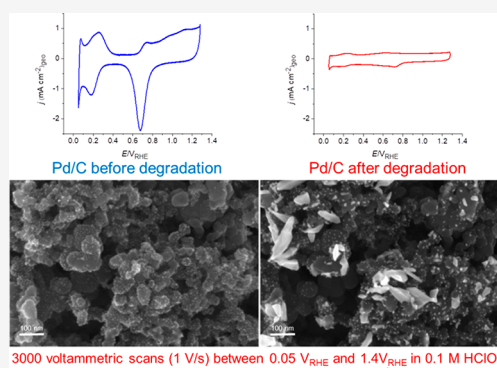
Read Online

ACCESS |

Metrics & More

Article Recommendations

**ABSTRACT:** Palladium has attracted significant attention as a catalyst or co-catalyst for many electrochemical reactions in energy conversion devices. We have studied electrochemical stability of a commercial Pd/C sample in an acidic electrolyte by exposing it to an accelerated stress test (AST) to mimic potential spikes in fuel cells and electrolyzers during start/stop events. AST consisted of extensive rapid potential cycling (5000 cycles, 1 V/s) in two potential regions, namely AST1 was performed between 0.4 and 1.4 V<sub>RHE</sub>, while AST2 was performed between 0.05 and 1.4 V<sub>RHE</sub>. Degradation of Pd/C was monitored by the changes in Pd electrochemical surface area, while the hydrogen evolution reaction (HER) was used as a test reaction to observe the corresponding impact of the degradation on the activity of Pd/C. Significant Pd/C degradation and HER activity loss were observed in both potential regions. Coupling of the electrochemical flow cell with an inductively coupled plasma mass spectrometry device showed substantial Pd dissolution during both ASTs. Identical location scanning electron microscopy revealed that Pd dissolution is followed by redeposition during both ASTs, resulting in particle size growth. Particle size growth was seen as especially dramatic in the case of AST2, when particularly large Pd nanostructures were obtained on top of the catalyst layer. According to the results presented in this work, (in)stability of Pd/C and other Pd-based nanocatalysts should be studied systematically as it may present a key factor limiting their application in energy conversion devices.



## 1. INTRODUCTION

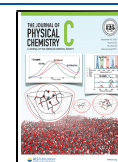
Palladium has attracted significant attention over the past decades as a catalytic material in energy conversion devices. Interest in Pd was initially driven by its chemical and physical similarities with Pt coupled with notably higher abundance in the Earth's crust and high electrocatalytic activity for different reactions. All together, these motivations highlighted Pd as a perfect substitute for scarce Pt. Pd-based materials were widely explored as catalysts for hydrogen evolution/oxidation reactions (HER/HOR).<sup>1,2</sup> HER has been studied on Pd nanoparticles loaded on various supports, Pd-alloys, Pd-bimetallics and Pd-intermetallics, as nicely reviewed in ref 1. Representative examples of Pd applications for HOR are studies concerning Pd–Pt alloys, where comparable or higher activity with respect to Pt/C benchmarks were obtained.<sup>2–5</sup> Another advantage of Pd-alloys (mainly Pd–Au and Pt–Pd) in HOR catalysis is higher tolerance toward CO poisoning than Pt,<sup>2,6</sup> which is very sensitive to the traces of CO present in the H<sub>2</sub> fuel. Regarding oxygen reduction reaction (ORR), the activity of Pd/C is in general five times lower than that of Pt/C in acid electrolyte;<sup>2,7</sup> nevertheless, Pd is the second most active metal for this reaction and provides complete 4e<sup>−</sup> reduction of oxygen to water. As in the case of Pt, alloying with transition

metals is a viable path to improve the activity of Pd catalysts for ORR. For instance, ternary Pd–Co–Mo<sup>8</sup> and Pd–Co–Pt catalysts<sup>9</sup> were reported as more active for ORR than Pt/C benchmarks. If Pd loadings are kept low, selectivity during ORR can be tuned from 4e<sup>−</sup> to 2e<sup>−</sup> reduction and H<sub>2</sub>O<sub>2</sub> production, which means that Pd is a promising catalyst for small scale on-site electrochemical synthesis of this valuable compound.<sup>10–12</sup> Another example of diverse Pd application is emerging electrochemical CO<sub>2</sub> reduction, where Pd nanoparticles were reported as efficient catalysts with high selectivity toward CO and formate production.<sup>13</sup> The most significant attention Pd-catalysts are gaining for the electro-oxidation of formic acid and alcohols.<sup>14</sup> Pd/C is a better catalyst for formic acid oxidation than Pt/C due to favorable reaction pathways that lead to the formation of minor amounts of CO, which acts as strongly adsorbed poisoning species and

Received: September 27, 2021

Revised: November 9, 2021

Published: December 10, 2021



blocks active surface sites.<sup>14</sup> Pd-based materials outperform Pt for the ethanol oxidation reaction,<sup>14–16</sup> especially in alkaline media. Overall, this brief literature survey shows high interest toward Pd application in low temperature fuel cells and electrolyzers, both in acidic and alkaline media. Depending on the demand, which dictates the fluctuating market price and supply of this critical raw material, the sustainability of its use as an electrocatalyst is hard to predict. Interestingly, at the moment palladium is notably more expensive than platinum (approximately 30 euro/g for Pt and 60 euro/g for Pd).

In addition to activity and economic viability, electrocatalytic materials must exhibit good stability to fulfill basic demands for application. In that regard, electrochemical dissolution of Pd has been studied in the past and first reports proposed that it takes place through anodic mechanism.<sup>17–19</sup>

On the contrary, many authors argued that Pd is electrochemically dissolved mainly during the reduction of previously formed Pd oxides.<sup>20,21</sup> A detailed study on this topic was performed recently by Pizzutilo et al. by using a setup consisting of an electrochemical scanning flow cell connected with the inductively coupled plasma mass spectrometry (ICP-MS) device,<sup>22</sup> which provided a potential-dependent dissolution profile of Pd in different acidic media. It was shown that the onset of Pd dissolution coincides with the oxidation of Pd surface and that depending on the upper potential limit (UPL), the dissolution profile of Pd contains up to three dissolution peaks, namely one anodic and two cathodic peaks. The anodic peak was connected with metallic Pd dissolution ongoing in parallel with Pd oxidation. The first cathodic peak, observed only at UPLs above 1.5  $V_{RHE}$ , was ascribed to the dissolution of Pd(IV)-oxide to produce  $Pd^{2+}$  ions detected by ICP-MS. The second cathodic peak was associated with the direct dissolution of Pd metal obtained by the reduction of Pd(II)-oxide, or alternatively by the dissolution of remaining Pd(IV)-oxide. The share of cathodic dissolution during the reduction of Pd-oxide becomes higher with the increase of UPL above 1.5  $V_{RHE}$ , while at lower UPLs anodic dissolution is predominant. Importantly, this work showed that Pd dissolves much more than Pt or Au under similar conditions, as well as that its dissolution in sulfuric acid is five times higher than in the perchloric acid. All of this was shown to be relevant for Pd/C as well,<sup>22</sup> meaning that degradation of real-life nanoparticulated Pd-based catalysts can be expected in energy conversion devices. Interestingly, despite substantial interest for Pd in electrocatalysis, only a few studies have been performed on this topic. Zadick et al. investigated stability of Pd/C by exposing the catalyst to a short stress test consisting of 150 cyclic voltammograms (CVs) recorded at a sweep rate of 100 mV/s in the potential region between 0.1 and 1.23  $V_{RHE}$  in both acid and alkaline media.<sup>23</sup> This quite mild stress test performed in 0.1 M  $H_2SO_4$  electrolyte provoked significant loss of the Pd electrochemical surface area (ESA), pointing out to the instability of real-life Pd nanocatalysts. However, there was no information about the extent of Pd dissolution or about the degradation mechanisms that occurred during the applied degradation protocol.<sup>23</sup> Another study was performed by Tang and colleagues by exposing Pd/C catalysts to the similar short degradation test in 0.5 M  $H_2SO_4$  electrolyte, which led to the significant decay of Pd ESA coupled with loss of electrocatalytic activity for ORR.<sup>24</sup> Rapid decay of the Pd ESA was also observed during slow scan CVs recorded in concentrated 2.5 M  $H_2SO_4$  electrolyte.<sup>25</sup> Kumar et al. have reported that anodic dissolution of Pd nanoparticles in acid media in the

presence of chlorides is largely promoted by the decrease of particle size.<sup>26</sup> It is important to note that all of these works were conducted in the conditions where Pd dissolution is strongly promoted, either in sulfuric acid solution as electrolyte<sup>23–25</sup> or in the presence of chlorides.<sup>26</sup>

The accelerated stress test (AST) is adopted as an effective method to screen the stability of electrocatalytic materials in laboratory conditions. AST implies exposing catalysts, usually in the form of thin-film deposited on rotating disc electrode, to a certain potentiodynamic or potentiostatic treatment and tracking the decrease of its ESA as a direct sign of catalyst deactivation. Degradation of Pt/C catalysts has been widely studied, owing to their pivotal role in fuel cells technology. As Pt is particularly sensitive to the dissolution and degradation during transitions between reduced and oxidized states of the surface,<sup>27,28</sup> ASTs were usually performed by extensive rapid potential cycling (scan rate such as 1 V/s) between low and high values (for instance between 0.05  $V_{RHE}$  up to 1.5  $V_{RHE}$ ), which corresponds to the conditions that appear during start/stop events in fuel cells.<sup>29–35</sup> Dissolution of Pt (and other metals of interest) under ASTs can be effectively monitored and quantified by coupling an electrochemical flow cell (EFC) with ICP-MS,<sup>31,35–39</sup> a method earlier developed in our group. Advanced characterization methods, such as identical location SEM (IL-SEM), were also developed and used in our group to understand local nanoscale degradation mechanisms caused by stress tests.<sup>34,37,40</sup> Therefore, the durability of Pd/C real-life catalyst should be investigated in a similar way as in the case of Pt/C, i.e. under the conditions relevant for applications in fuel cells/electrolyzers, and corresponding degradation mechanisms should be exposed.

In the present contribution, we have studied the electrochemical stability and degradation mechanisms of a commercial Pd/C catalyst by subjecting it to AST consisting of 5000 rapid voltammetric scans (1 V/s) in 0.1 M  $HClO_4$  in two potential regions, namely 0.4–1.4  $V_{RHE}$  and 0.05–1.4  $V_{RHE}$ . The purpose of different lower potential limits is to investigate the effect of potential window on the stability and degradation mechanism of Pd/C, as different conditions may appear in the energy conversion devices during stable running and during switching on/off. Degradation of Pd/C during ASTs was tracked by the decay of Pd ESA and by corresponding changes in the reactivity of Pd/C for HER, which was used as the test reaction. Pd dissolution under the conditions applied in ASTs was monitored by setup consisting of EFC coupled with ICP-MS (EFC-ICP-MS). Nanoscale degradation mechanism of Pd/C was revealed by IL-SEM imaging taken before, during and after ASTs.

## 2. METHODS

Pd/C commercial catalyst with 20 wt % Pd on carbon was provided by Premetek. Catalyst ink was prepared by mixing 1 mL of Milli-Q water with 1 mg of Pd/C powder. To obtain finely dispersed catalyst ink, the mixture was placed in ice-cooled ultrasonic bath for minimum 15 min. Rotating disc electrodes (RDEs) made of glassy carbon (GC) discs (5 mm in diameter) embedded in Teflon holders were used as working electrodes. GC RDEs were hand-polished with 0.05  $\mu m$  alumina paste followed by removal of alumina residues in Milli-Q water in ultrasonic bath. Pd/C thin films (TFs) were prepared by drop-casting 20  $\mu L$  of the Pd/C catalyst suspension onto the RDE surface directly from an ultrasonic bath to ensure good dispersion. Electrodes were placed in a

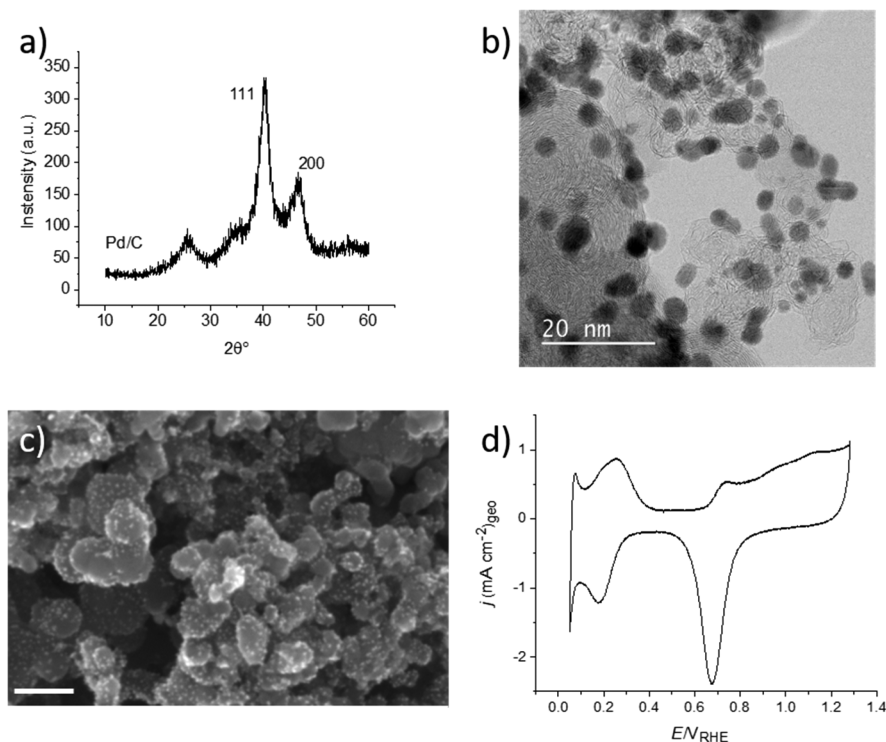


**Figure 1.** Characterization of Pd/C catalyst: (a) XRD spectrum; (b) TEM imaging; (c) SEM imaging (scale bar corresponds to 100 nm); (d) cyclic voltammogram of Pd/C (0.1 M HClO<sub>4</sub>, 50 mV/s).

desiccator box to avoid contamination and to allow slow drying to obtain homogeneous catalyst films. Afterward, films were covered with 5  $\mu$ L of Nafion (5 wt % in mixture of lower aliphatic alcohols and water, Sigma-Aldrich) solution in isopropanol (1:50) to provide good adhesion.

The cleanliness of the electrochemical cell and all accompanying glassware was maintained by boiling in distilled water followed by extensive rinsing with Milli-Q water before and after each experiment. Electrochemical measurements were conducted in a three electrode setup, with a thin Pd/C film covered RDE (TF-RDE) as the working electrode. Glassy carbon rod was used as a counter electrode rather than Pt or Au to avoid possible contamination of the electrolyte by the dissolution of these metals. The reference Ag/AgCl electrode was separated from the main cell compartment by an electrolytic bridge to eliminate possible chloride leakage into the electrolyte, as it would have an important impact on the stability tests. All potentials in this work are given with respect to a reversible hydrogen electrode (RHE).

ASTs were performed in 0.1 M HClO<sub>4</sub> electrolyte prepared by mixing the appropriate amounts of concentrated perchloric acid (Rotipuran Supra 70%, Carl Roth) and Milli-Q water. Rapid electrochemical activation of Pd/C samples was used to ensure electrolyte penetration into catalyst layer and to reach stable voltammetric response. Activation consisted of 10 CVs taken at a sweep rate of 300 mV/s in the potential region 0.05–1.28 V<sub>RHE</sub>, followed by two slow scan CVs (50 mV/s) in the same potential region, which were used as the baseline for the following degradation studies. HER polarization curves were then collected at a scan rate of 10 mV/s in the potential range between 0.2 and –0.1 V<sub>RHE</sub>. AST consisted of 5000 rapid CV scans (1 V/s) in two different potential regions: AST1 was performed in potential window 0.4–1.4 V<sub>RHE</sub>, while AST2 was performed in the potential region 0.05–1.4 V<sub>RHE</sub>. At

every 1000 scans, a pair of control slow scan CVs and HER polarization curves were recorded to monitor the progress of degradation.

Characterization of pristine Pd/C powder by XRD was performed on a PANalytical X'Pert PRO MPD (PANalytical B.V., Almelo, The Netherlands) device with a Cu K $\alpha$ 1 radiation ( $\lambda$  = 1.5406 Å) in the  $\alpha$ 1 configuration with a Johansson monochromator on the primary side. The diffractograms were recorded with 0.034° resolution and 100 s signal integration time in the  $2\theta$  range from 10 to 60°. For TEM imaging (JEOL JEM-ARM200CF, Ltd., Tokyo, Japan operated at 80 kV), initial Pd/C suspension was diluted 10 times with Milli-Q water and 5  $\mu$ L of resulting catalyst ink was drop-casted onto TEM grid. IL-SEM images of the Pd/C sample before, during, and after both ASTs were acquired on field-emission scanning electron microscope (Supra 35 V, Carl Zeiss, Germany). GC electrodes with deposited Pd/C film were mounted onto SEM stage via dedicated homemade holder that provides electrical contact between stage and glassy carbon tip.

The EFC-ICP-MS system for the potential resolved analysis of the dissolved metals is described in detail in our previous works.<sup>38,41</sup> Briefly, setup consists of an EFC, which is custom-made from polyether ether ketone (PEEK) based on a design of a commercial cell (cross-flow cell, BASi), connected to an ICP-MS instrument (Agilent 7900, Agilent Technologies), equipped with a MicroMist glass concentric nebulizer and a Peltier cooled Scott-type double-pass quartz spray chamber. The electrolyte flow at a constant rate of 400  $\mu$ L/min was set in the direction from the counter electrode toward the working electrode with a mechanical syringe pump. Glassy carbon discs (3 mm diameter) embedded into the PEEK material of EFC (ALS dual-type electrode for cross-flow cell, 25 mm  $\times$  25 mm) served as the working and counter electrode. They were



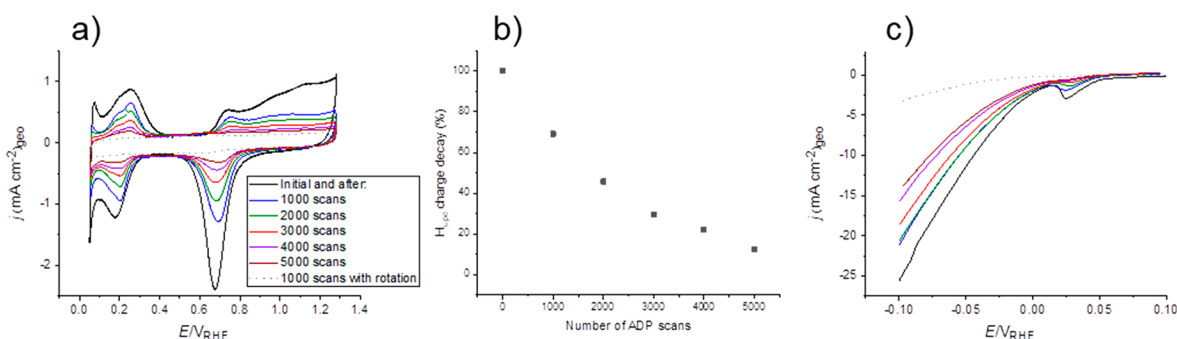


**Figure 2.** AST1 performed by potential cycling (1 V/s) in the range between 0.4 and 1.4  $V_{\text{RHE}}$  in 0.1 M  $\text{HClO}_4$ : (a) CVs for monitoring the loss of Pd ESA (50 mV/s); (b) corresponding decay of Pd ESA calculated from  $H_{\text{upd}}$  charge; (c) corresponding HER polarization curves (10 mV/s).

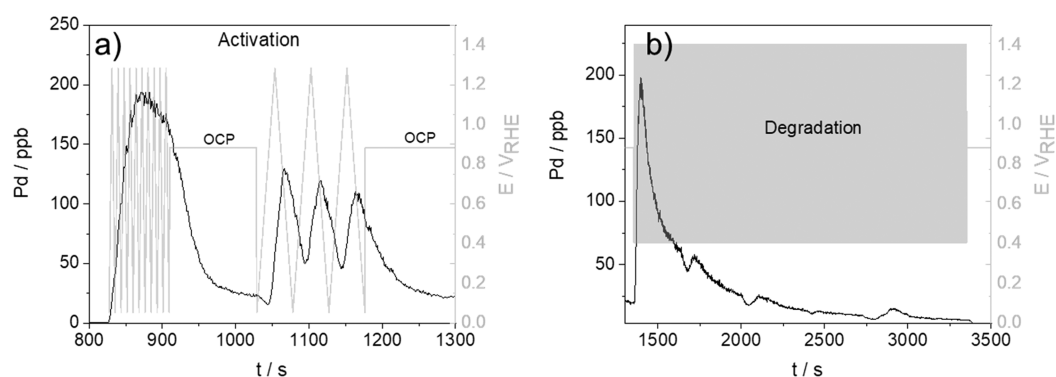


**Figure 3.** EFC-ICP-MS results of Pd dissolution during AST1: (a) electrochemical activation of the Pd/C; (b) 1000 rapid AST1 scans (1 V/s) in the potential region 0.4 and 1.4  $V_{\text{RHE}}$ . OCP periods were applied before and after activation to ensure stabilization of Pd dissolution signal.

cleaned in the same way as described above for RDE GC electrodes. The Pd/C catalyst suspension (1 mg/mL) was coated (5  $\mu\text{L}$ ) on one of the GC disks and left to dry slowly under ambient conditions. An Ag/AgCl reference electrode with a ceramic frit (MW-2030, BASi) was used as a reference electrode, and its potential was previously determined versus a RHE in a RDE setup. The standardization curve was determined based on the standard solutions containing 1, 2, 5, 10, 20, 50, and 100 ppb of Pd.

### 3. RESULTS AND DISCUSSION

#### 3.1. Characterization of Pristine Pd/C Catalyst.

Characterization of the commercial Pd/C material (20 wt %, Premetek) used in this work is presented in Figure 1. The diffraction pattern of Pd/C, given in Figure 1a, contains peak at  $25.3^\circ$  corresponding to graphite (200) planes of carbon support, while peaks at  $40.3^\circ$  and  $46.4^\circ$  correspond to the (111) and (200) reflections of the face centered cubic lattice of Pd (JCPDS card no. 05-0681).

TEM imaging, given in Figure 1b, shows that Pd/C sample contains uniform-sized Pd nanoparticles, the majority of which have a diameter in the range between 2 and 6 nm (particle size distribution not shown). It should be mentioned that particle agglomeration has been observed randomly, but not frequently. SEM imaging of Pd/C catalyst deposited on glassy carbon in the TF-RDE setup, Figure 1c, confirm the properties observed in TEM imaging. Cyclic voltammogram of Pd/C, Figure 1d, was obtained after short electrochemical activation in 0.1 M  $\text{HClO}_4$  electrolyte and used as the baseline for the following degradation studies. All well-known electrochemical features of palladium nanoparticles in acid media can be seen.<sup>22</sup> At more negative potentials than 0.1  $V_{\text{RHE}}$ , electro-

sorption of hydrogen into Pd nanoparticles takes place,<sup>42,43</sup> as can be seen by the current drop in the negative going scan and its counterpart at positive going scan due to desorption.  $H_{\text{upd}}$  peaks appear at potentials between 0.1 and 0.40  $V_{\text{RHE}}$  followed by the double layer region at more positive potentials. Since  $H_{\text{upd}}$  and hydrogen electrosorption are well-separated in the case of Pd nanoparticles,<sup>42,43</sup> charge corresponding to the  $H_{\text{upd}}$  process will be used to track the ESA of the Pd/C during degradation.<sup>44</sup> In the forward scan, Pd oxidation commences at potentials around 0.60  $V_{\text{RHE}}$ , while the corresponding Pd-oxide reduction peak is centered at around 0.68  $V_{\text{RHE}}$  in the backward sweep.

**3.2. Accelerated Stress Test 1: Potential Region 0.4–1.4  $V_{\text{RHE}}$ .** AST1 was performed by subjecting the Pd/C catalyst to 5000 rapid CV scans (1 V/s) in the 0.1 M  $\text{HClO}_4$  electrolyte in the potential window 0.4–1.4  $V_{\text{RHE}}$ . Results showing the impact of AST1 on the electrochemistry of Pd/C are given in Figure 2.

Comparison of the CVs taken periodically during AST1, given in Figure 2a, clearly points out the significant degradation of the Pd/C. To quantify degradation, the Pd ESA was estimated Figure 2a by calculating the charge corresponding to  $H_{\text{upd}}$  peaks.<sup>44</sup> Significant degradation of Pd/C is illustrated in Figure 2b by the progressive decay of Pd ESA to only 11% of the initial value at the end of the degradation test. Polarization curves for HER collected during AST1 are given in Figure 2c. A voltammetric peak in the potential range between 0.1 and 0.015  $V_{\text{RHE}}$  corresponds to the hydrogen electrosorption into Pd nanoparticles,<sup>42,43</sup> while HER commences and proceeds at more negative potentials. Clearly, both HER activity and hydrogen electrosorption are impacted by degradation during AST1 in the same fashion.



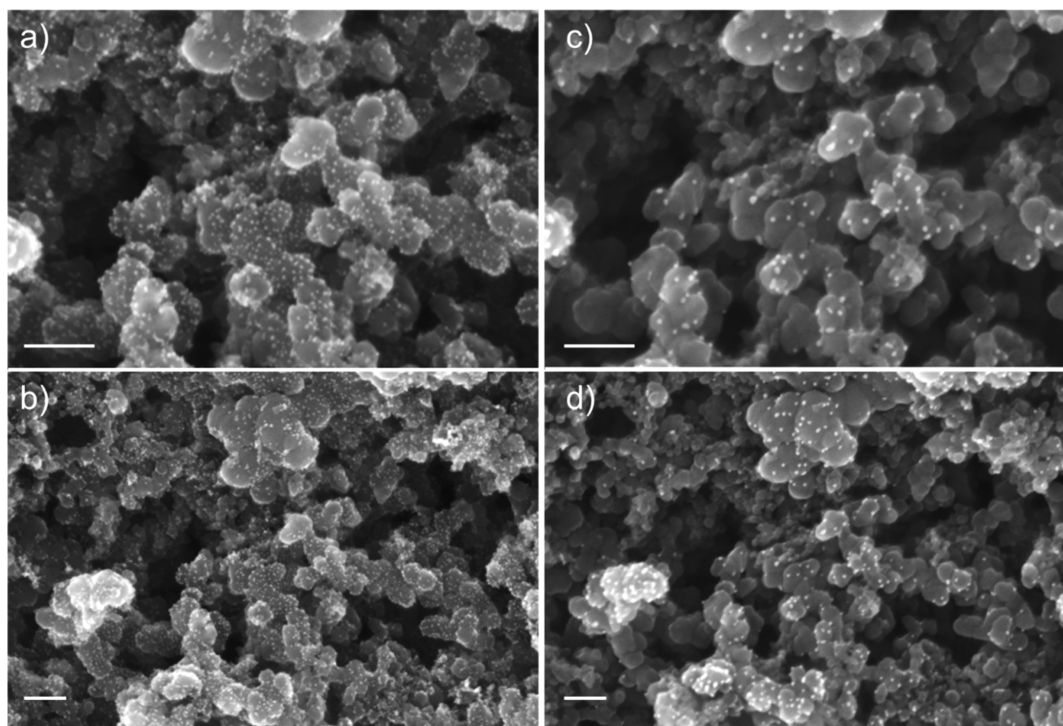


**Figure 4.** IL-SEM imaging of the Pd/C sample: (a,b) before and (c,d) after AST1 (0.1 M HClO<sub>4</sub>, 5000 scans at 1 V/s, potential range between 0.4 and 1.4 V<sub>RHE</sub>). Scale bars correspond to 100 nm.

The extent of Pd dissolution from Pd/C during AST1 was studied using EFC-ICP-MS setup, and obtained results are presented in Figure 3. The protocol was the same as in the TF-RDE setup, and it included short activation followed by 1000 rapid AST1 scans, with OCP periods between to provide stabilization of the ICP-MS signal. Activation of the Pd/C, given in Figure 3a, already led to rather substantial dissolution since 7.1% of the total Pd mass from the catalytic layer is leached in the electrolyte flow. To illustrate how significant this is, one should note that in the case of Pt/C and Rh/C catalysts used in our previous studies (unpublished results), the amount of metals dissolved during (even longer) activation procedures was calculated to 0.38% and 0.025%, respectively. Having this in mind, we should also note that recording of the slow scan CVs for tracking of Pd ESA (given in Figure 2a) after each 1000 AST1 cycles brings additional stress to the Pd/C material; however, degradation caused by prolonged AST should still be dominant. In any case, significant Pd dissolution from Pd/C during very short electrochemical activation already puts a question mark on the usage of Pd/C in energy conversion devices.

EFC-ICP-MS analysis of Pd dissolved during the first 1000 rapid AST1 scans is given in Figure 3b. Occasional spikes in the dissolution profile most likely originate from the formation of the microbubbles due to the high scan rate (1 V/s) and correspondingly high currents at both working and counter electrodes. In the first 1000 AST1 scans, around 53% of Pd mass left in the sample after activation is detected in the electrolyte stream by ICP-MS, Figure 3b. Corresponding ESA decay in TF-RDE setup is around 31% (Figure 2b). This difference could originate from different hydrodynamic conditions during measurements in TF-RDE and EFC setups. Namely, electrolyte flow in EFC-ICP-MS setup promotes mass transport of dissolved Pd species from the catalyst layer and

prevents or reduces the possibility for redeposition, which is common degradation mechanism for nanoparticulated catalysts.<sup>45</sup> In the case of TF-RDE setup, no electrode rotation was applied and hence the probability of redeposition of dissolved Pd species is higher than in EFC setup. To check this hypothesis, AST1 in TF-RDE setup was performed under electrode rotation at 1600 rpm, which resulted in extremely fast degradation. After only 1000 AST1 scans practically no Pd features are visible in the corresponding CV (see Figure 2a, dotted gray line). Such rapid degradation is followed by the accordingly significant decay of HER activity (see Figure 2c, dotted gray line). Under rotation, mass transport of dissolved Pd is enhanced and catalyst degradation by dissolution is more dramatic, while redeposition is suppressed. Therefore, a direct correlation between results of AST1 in TF-RDE and in EFC-ICP-MS setups cannot be drawn; however, they do confirm substantial Pd/C degradation.

Local morphological nanoscale changes in the Pd/C sample were visualized by IL-SEM imaging before and after AST1 to expose degradation mechanism. IL-SEM images, given in Figure 4, show quite significant degradation of the Pd/C at the end of applied stress test, which is in agreement with results obtained in TF-RDE and EFC-ICP-MS setups.

Top panel IL-SEM images (Figures 4a,c) were taken at higher magnification, and it can be seen that AST1 led to the two significant changes: (i) a substantial amount of Pd nanoparticles is absent and (ii) the appearance of up to a two to three times larger Pd particles. The same features can be seen in bottom panel images taken at lower magnifications (Figures 4b,d), meaning that degradation is uniform across the catalyst film. Since we showed earlier that both dissolution and redeposition are involved in degradation, it can be concluded that observed particle growth is a consequence of the so-called 3D Ostwald ripening.<sup>45,46</sup> This degradation mechanism,

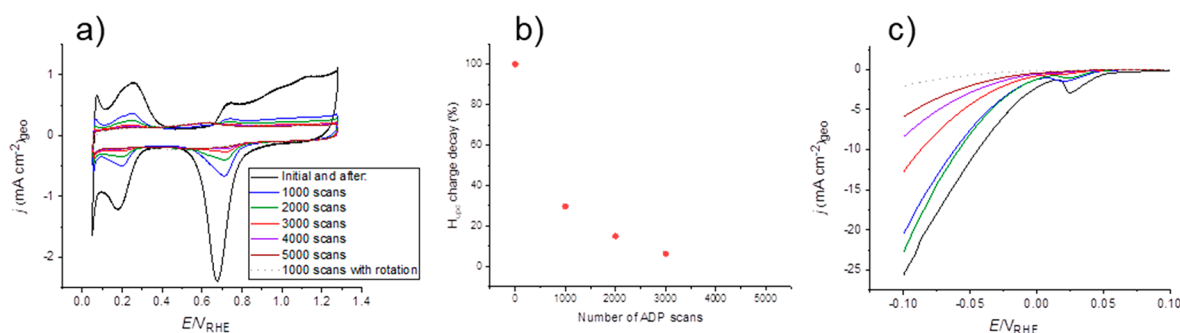


**Figure 5.** AST2 performed by potential cycling (1 V/s) in the range between 0.05 and 1.4  $V_{\text{RHE}}$  in 0.1 M  $\text{HClO}_4$ : (a) CVs for monitoring of the loss of Pd ECSA (50 mV/s); (b) corresponding decay of Pd ESA calculated from  $H_{\text{upd}}$  peaks charge; and (c) corresponding HER polarization curves (10 mV/s).

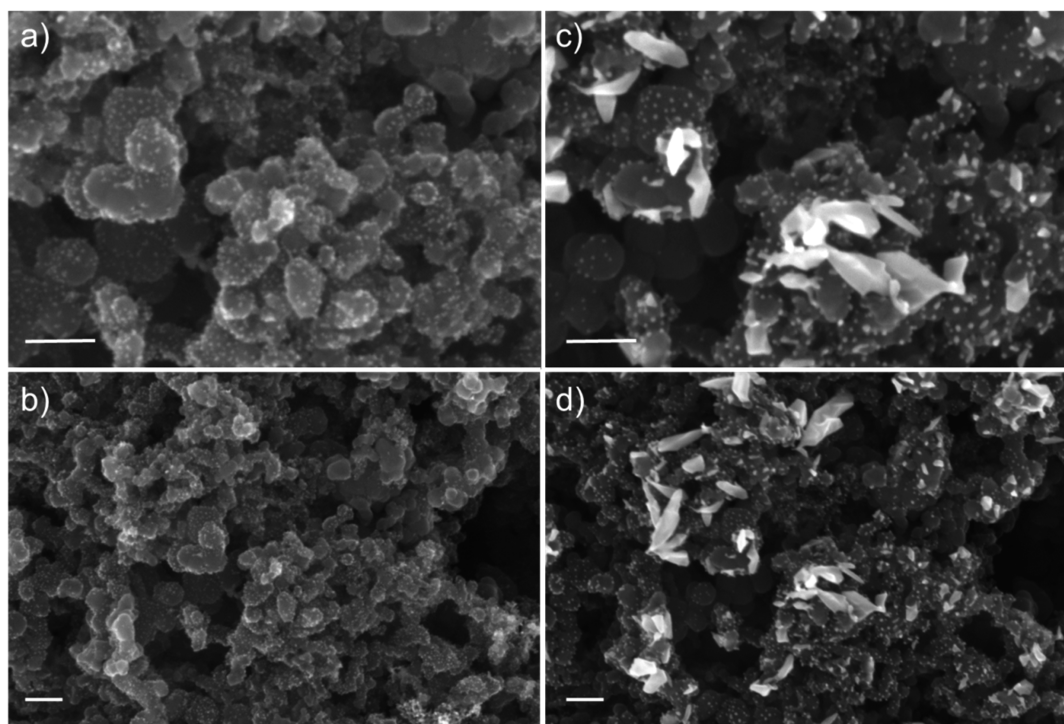


**Figure 6.** IL-SEM imaging of the Pd/C sample: (a,b) before and (c,d) after 3000 AST2 scans (0.1 M  $\text{HClO}_4$ , 1 V/s, potential range between 0.05 and 1.4  $V_{\text{RHE}}$ ). Scale bars correspond to 100 nm.

otherwise common for Pt/C catalysts,<sup>34,45,46</sup> proceeds *via* dissolution of nanoparticles in the electrolyte followed by redeposition. Smaller particles in the sample are more prone to dissolution than larger ones,<sup>37,45–47</sup> while redeposition preferentially occurs on larger particles as these are energetically more favorable.<sup>34,45</sup> Overall, IL-SEM imaging complies well with TF-RDE and EFC-ICP-MS results, which all together show that degradation of Pd/C during AST1 proceeds *via* dissolution followed by redeposition.

**3.3. Accelerated Stress Test 2: Potential Region 0.05–1.4  $V_{\text{RHE}}$ .** To check the influence of the lower potential limit on the degradation of Pd/C, AST2 was performed in the potential region between 0.05 and 1.4  $V_{\text{RHE}}$  and results obtained in TF-RDE setup are given in Figure 5. Such fast spikes between low and high potentials are often encountered in fuel cells and electrolyzers during switching on/off and are known to be particularly damaging for Pt/C catalysts. In this case, rather severe degradation of Pd/C occurs as can be seen in Figure 5a by fast decline of Pd features in the CVs taken

during AST2. Pd ESA decays rapidly, as evident from Figure 5b. After only 3000 AST2 scans,  $H_{\text{upd}}$  peaks are barely visible and cannot be integrated in a precise manner, as well as Pd-oxide reduction peak, however, their presence means that Pd is not completely degraded from the catalyst layer. Corresponding impact of the degradation during AST2 on HER reactivity (and hydrogen electrosorption) is evident from Figure 5c.

The amount of Pd dissolved during 1000 AST2 scans calculated from EFC-ICP-MS (data not shown) was practically equal to the amount of Pd dissolved during AST1 (within a few percent difference). This was to a certain extent expected, as changing the lower potential limit to a more negative value should not result with higher transient Pd dissolution, since both used lower potential limits provide full reduction of Pd-oxide. The impact of rotation on degradation during AST2 is in accordance with AST1 (see dotted gray lines in Figure 5a and c), confirming the influence of mass transport of dissolved Pd species onto degradation. Therefore, it is reasonable to assume that redeposition of Pd is more effective at lower

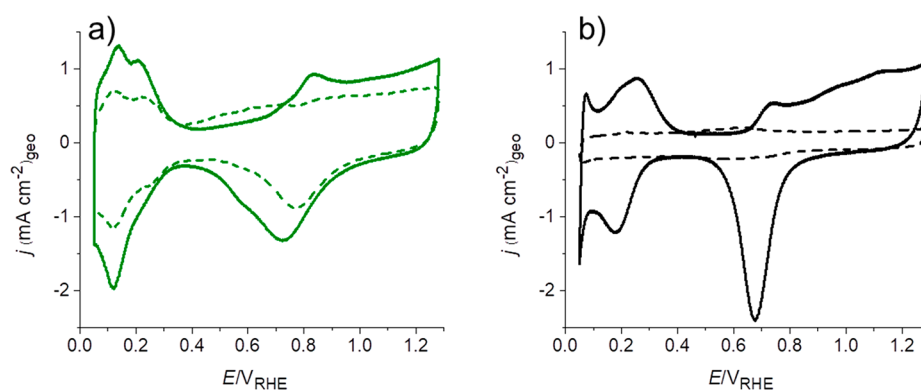


**Figure 7.** Comparison of the degradation of Pt/C and Pd/C catalysts during AST2 (0.1 M HClO<sub>4</sub>, 3000 scans at 1 V/s, 0.05–1.4 V<sub>RHE</sub>). Presented CVs are recorded in 0.1 M HClO<sub>4</sub> electrolyte in the potential range 0.05–1.28 V<sub>RHE</sub> at a scan rate of 50 mV/s before (full lines) and after (dashed lines) degradation test. Loadings of Pt and Pd were adjusted to 5 and 4 μg, respectively.

potentials applied in AST2 and responsible for more pronounced Ostwald ripening and thus more pronounced ESA decay.

To visualize Pd/C degradation on the nanoscale level during AST2, IL-SEM was performed before and after 3000 degradation cycles and collected images are presented in Figure 6. Top panel IL-SEM imaging (Figures 6a,c) taken at higher magnifications shows that Pd/C degradation during AST2 results in a pronounced growth of nanoparticles and particularly large Pd-nanocrystals. This growth seems to occur predominantly on top of the catalysts layer, while a significant portion of Pd particles appears missing from the depth of the sample. Bottom panel IL-SEM images with lower magnification (Figure 6b,d) show that degradation is uniform across the catalyst film. IL-SEM confirms that degradation occurs *via* dissolution of Pd particles, followed by redeposition back onto the outer layer of the catalyst film. Similar phenomena of 3D Ostwald ripening with the growth of big metallic crystals were already observed for the case of Pt/C, however only after prolonged potential cycling (50 000 scans).<sup>34</sup>

To summarize presented results, significant Pd/C degradation occurs during stress tests in both used potential regions in 0.1 M HClO<sub>4</sub> electrolyte, namely 0.4–1.4 V<sub>RHE</sub> and 0.05–1.4 V<sub>RHE</sub>. Substantial and fast decay of Pd ESA followed by the corresponding drop of the HER activity were obtained in the TF-RDE setup, while the EFC-ICP-MS setup detected significant Pd dissolution. IL-SEM revealed that dissolution was followed by redeposition and particle size growth in the TF-RDE setup. Redeposition was more pronounced for AST2, i.e. when lower potential limit was applied, as particularly large Pd nanostructures were formed on top of the catalyst layer.

Since Pd is regarded as a possible substitute for Pt in fuel cells and electrolyzers, it is interesting to compare the results obtained in this work with the stability of Pt/C benchmark. Electrochemical stability of 20 wt % Pt/C (Premetek) was studied by exposing the catalyst to a protocol corresponding to AST2 and comparison with Pd/C degradation is shown in Figure 7. It is obvious that both catalysts suffer deactivation, however degradation of Pd/C is clearly much more dramatic than that of Pt/C.

Calculated from the H<sub>upd</sub> charge, the Pt ESA dropped down to 62.5% of the initial value at the end of the degradation test, Figure 7a. In the case of Pd/C, the ESA dramatically dropped down to only 6.5% of the initial value, Figure 7b. Even if Pd may be a suitable substitute for Pt from the activity point of

view, the comparison given in Figure 7 clearly shows that Pd/C is much more susceptible to degradation than Pt/C when subjected to harsh transient start/stop conditions in energy conversion devices. Another motivation for Pd application came from its significantly lower cost in the past with respect to Pt combined with higher abundance. However, the trend in the prices of Pt and Pd has been slowly changing in the past decade, and since the middle of 2017, it has reversed. At the moment, Pd is around two times more expensive than Pt.<sup>49</sup> Having all that in mind, in order to sustainably use expensive Pd for electrocatalytic purposes, special attention must be devoted to their non-satisfactory stability and strategies to enhance it. For example, it was shown that implementation of Au in Pt fuel cell catalysts can promote their durability while preserving the activity;<sup>32,48</sup> hence similar strategies can be explored in order to provide active and stable Pd-based nanocatalysts. Therefore, the stability of Pd-based catalysts should be taken into account and studied systematically for each particular case of their possible usage; for example, in both acid and alkaline electrolytes, in the potentiostatic and potentiodynamic conditions, etc.

#### 4. CONCLUSIONS

In the present contribution, we have demonstrated high electrochemical instability and rapid degradation of a commercial Pd/C catalyst by exposing it to AST in the acidic electrolyte (0.1 M HClO<sub>4</sub>) in two different potential regions. In the AST1 performed in potential window 0.4–1.4 V<sub>RHE</sub>, significant decay of Pd ESA was observed and coupled with the loss of HER activity, which was used as a test reaction in this study. EFC-ICP-MS analysis showed significant Pd dissolution during AST1, while IL-SEM revealed that dissolution followed by redeposition is the main degradation mechanism. As for AST2, performed in the potential region 0.05–1.4 V<sub>RHE</sub>, even faster degradation was observed in the TF-RDE setup, while the amount of dissolved Pd detected in EFC-ICP-MS was equal as in AST1. IL-SEM revealed that redeposition was additionally promoted at lower applied potentials in AST2, leading to the formation of particularly large Pd nanostructures on the top of the catalyst layer. Results presented in our contribution emphasize the importance of systematic study of the durability of nanoparticulated Pd catalysts, since it may present a limiting factor for their application in energy conversion devices.



## ■ AUTHOR INFORMATION

## Corresponding Authors

**Milutin Smiljanić** – Department of Materials Chemistry, National Institute of Chemistry, 1000 Ljubljana, Slovenia; Laboratory for Atomic Physics, Institute for Nuclear Sciences Vinča, University of Belgrade, 11001 Belgrade, Serbia; [orcid.org/0000-0002-4911-5349](https://orcid.org/0000-0002-4911-5349); Email: [milutin.smiljanic@ki.si](mailto:milutin.smiljanic@ki.si)

**Nejc Hodnik** – Department of Materials Chemistry, National Institute of Chemistry, 1000 Ljubljana, Slovenia; Jožef Stefan International Postgraduate School, 1000 Ljubljana, Slovenia; University of Nova Gorica, 5000 Nova Gorica, Slovenia; [orcid.org/0000-0002-7113-9769](https://orcid.org/0000-0002-7113-9769); Email: [nejc.hodnik@ki.si](mailto:nejc.hodnik@ki.si)

## Authors

**Marjan Bele** – Department of Materials Chemistry, National Institute of Chemistry, 1000 Ljubljana, Slovenia

**Leonard Moriau** – Department of Materials Chemistry, National Institute of Chemistry, 1000 Ljubljana, Slovenia; Jožef Stefan International Postgraduate School, 1000 Ljubljana, Slovenia

**Francisco Ruiz-Zepeda** – Department of Materials Chemistry, National Institute of Chemistry, 1000 Ljubljana, Slovenia

**Martin Sala** – Department of Analytical Chemistry, National Institute of Chemistry, 1000 Ljubljana, Slovenia; [orcid.org/0000-0001-7845-860X](https://orcid.org/0000-0001-7845-860X)

Complete contact information is available at: <https://pubs.acs.org/10.1021/acs.jpcc.1c08496>

## Notes

The authors declare no competing financial interest.

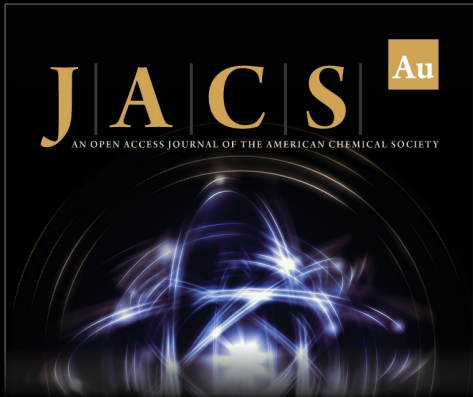
## ■ ACKNOWLEDGMENTS

This work was supported by the Ministry of Education, Science and Sport of the Republic of Slovenia through Raziskovalci-2.1-KI-952007 and by the Slovenian Research Agency through the research programs P1-0034 and P2-0393 and project N2-0106.


## ■ REFERENCES


- (1) Sarkar, S.; Peter, S. C. An Overview on Pd-Based Electrocatalysts for the Hydrogen Evolution Reaction. *Inorg. Chem. Front.* **2018**, *5*, 2060.
- (2) Shao, M. Palladium-Based Electrocatalysts for Hydrogen Oxidation and Oxygen Reduction Reactions. *J. Power Sources* **2011**, *196*, 2433–2444.
- (3) Cho, Y. H.; Choi, B.; Cho, Y. H.; Park, H. S.; Sung, Y. E. Pd-Based PdPt(19:1)/C Electrocatalyst as an Electrode in PEM Fuel Cell. *Electrochem. Commun.* **2007**, *9*, 378–381.
- (4) Escudero, M. J.; Hontañón, E.; Schwartz, S.; Boutonnet, M.; Daza, L. Development and Performance Characterisation of New Electrocatalysts for PEMFC. *J. Power Sources* **2002**, *106*, 206–214.
- (5) Grigoriev, S. A.; Lyutikova, E. K.; Martemianov, S.; Fateev, V. N. On the Possibility of Replacement of Pt by Pd in a Hydrogen Electrode of PEM Fuel Cells. *Int. J. Hydrogen Energy* **2007**, *32*, 4438–4442.
- (6) Kadirgan, F.; Kannan, A. M.; Atilan, T.; Beyhan, S.; Ozenler, S. S.; Suzer, S.; Yörür, A. Carbon Supported Nano-Sized Pt–Pd and Pt–Co Electrocatalysts for Proton Exchange Membrane Fuel Cells. *Int. J. Hydrogen Energy* **2009**, *34*, 9450–9460.
- (7) Shao, M. H.; Sasaki, K.; Adzic, R. R. Pd-Fe Nanoparticles as Electrocatalysts for Oxygen Reduction. *J. Am. Chem. Soc.* **2006**, *128*, 3526–3527.
- (8) Raghuveer, V.; Manthiram, A.; Bard, A. J. Pd-Co-Mo Electrocatalyst for the Oxygen Reduction Reaction in Proton Exchange Membrane Fuel Cells. *J. Phys. Chem. B* **2005**, *109*, 22909–22912.
- (9) Mathiyarasu, J.; Phani, K. L. N. Carbon-Supported Palladium-Cobalt-Noble Metal (Au, Ag, Pt) Nanocatalysts as Methanol Tolerant Oxygen-Reduction Cathode Materials in DMFCs. *J. Electrochem. Soc.* **2007**, *154*, 1100–1105.
- (10) Fortunato, G. V.; Pizzutilo, E.; Mingers, A. M.; Kasian, O.; Cherevko, S.; Cardoso, E. S. F.; Mayrhofer, K. J. J.; Maia, G.; Ledendecker, M. Impact of Palladium Loading and Interparticle Distance on the Selectivity for the Oxygen Reduction Reaction toward Hydrogen Peroxide. *J. Phys. Chem. C* **2018**, *122*, 15878–15885.
- (11) Ledendecker, M.; Pizzutilo, E.; Malta, G.; Fortunato, G. V.; Mayrhofer, K. J. J.; Hutchings, G. J.; Freakley, S. J. Isolated Pd Sites as Selective Catalysts for Electrochemical and Direct Hydrogen Peroxide Synthesis. *ACS Catal.* **2020**, *10*, 5928–5938.
- (12) Fortunato, G. V.; Pizzutilo, E.; Cardoso, E. S. F.; Lanza, M. R. V.; Katsounaros, I.; Freakley, S. J.; Mayrhofer, K. J. J.; Maia, G.; Ledendecker, M. The Oxygen Reduction Reaction on Palladium with Low Metal Loadings: The Effects of Chlorides on the Stability and Activity towards Hydrogen Peroxide. *J. Catal.* **2020**, *389*, 400–408.
- (13) Gao, D.; Zhou, H.; Cai, F.; Wang, J.; Wang, G.; Bao, X. Pd-Containing Nanostructures for Electrochemical CO<sub>2</sub> Reduction Reaction. *ACS Catal.* **2018**, *8*, 1510–1519.
- (14) Meng, H.; Zeng, D.; Xie, F. Recent Development of Pd-Based Electrocatalysts for Proton Exchange Membrane Fuel Cells. *Catalysts* **2015**, *5*, 1221–1274.
- (15) Chen, Y. X.; Lavacchi, A.; Chen, S. P.; Di Benedetto, F.; Bevilacqua, M.; Bianchini, C.; Fornasiero, P.; Innocenti, M.; Marelli, M.; Oberhauser, W.; et al. Electrochemical Milling and Faceting: Size Reduction and Catalytic Activation of Palladium Nanoparticles. *Angew. Chem., Int. Ed.* **2012**, *51*, 8500–8504.
- (16) Akhairi, M. A. F.; Kamarudin, S. K. Catalysts in Direct Ethanol Fuel Cell (DEFC): An Overview. *Int. J. Hydrogen Energy* **2016**, *41*, 4214–4228.
- (17) Rand, D. A. J.; Woods, R. A Study of the Dissolution of Platinum, Palladium, Rhodium and Gold Electrodes in 1 m Sulphuric Acid by Cyclic Voltammetry. *J. Electroanal. Chem. Interfacial Electrochem.* **1972**, *35*, 209–218.
- (18) Juodkasis, K.; Juodkazyte, J.; Šebeka, B.; Stalnionis, G.; Lukinskas, A. Anodic Dissolution of Palladium in Sulfuric Acid: An Electrochemical Quartz Crystal Microbalance Study. *Russ. J. Electrochem.* **2003**, *39*, 954–959.
- (19) Vracar, L. M.; Sepa, D. B.; Damjanovic, A. Palladium Electrode in Oxygen Saturated Solutions: Rest Potentials in Solutions of Different PH. *J. Electrochem. Soc.* **1987**, *134*, 1695.
- (20) Grdeň, M.; Łukaszewski, M.; Jerkiewicz, G.; Czerwiński, A. Electrochemical Behaviour of Palladium Electrode: Oxidation, Electrodeposition and Ionic Adsorption. *Electrochim. Acta* **2008**, *53*, 7583–7598.
- (21) Shrestha, R.; Nishikata, A.; Tsuru, T. Electrochimica Acta Channel Flow Double Electrode Study on Palladium Dissolution during Potential Cycling in Sulfuric Acid Solution. *Electrochim. Acta* **2012**, *70*, 42–49.
- (22) Pizzutilo, E.; Geiger, S.; Freakley, S. J.; Mingers, A.; Cherevko, S.; Hutchings, G. J.; Mayrhofer, K. J. J. Palladium Electrodeposition from Model Surfaces and Nanoparticles. *Electrochim. Acta* **2017**, *229*, 467–477.
- (23) Zadick, A.; Dubau, L.; Demirci, U. B.; Chatenet, M. Effects of Pd Nanoparticle Size and Solution Reducer Strength on Pd/C Electrocatalyst Stability in Alkaline Electrolyte. *J. Electrochem. Soc.* **2016**, *163*, F781.
- (24) Tang, Y.; Mu, S.; Yu, S.; Zhao, Y.; Wang, H.; Gao, F. In Situ and Ex Situ Studies on the Degradation of Pd/C Catalyst for Proton Exchange Membrane Fuel Cells. *J. Fuel Cell Sci. Technol.* **2014**, *11*, 1–7.


- (25) Wells, P. P.; Crabb, E. M.; King, C. R.; Wiltshire, R.; Billsborrow, B.; Thompson, D.; Russell, A. E. Preparation, Structure, and Stability of Pt and Pd Monolayer Modified Pd and Pt Electrocatalysts. *Phys. Chem. Chem. Phys.* **2009**, *11*, 5773–5781.
- (26) Kumar, A.; Buttry, D. A. Size-Dependent Anodic Dissolution of Water-Soluble Palladium Nanoparticles. *J. Phys. Chem. C* **2013**, *117*, 26783–26789.
- (27) Cherevko, S.; Keeley, G. P.; Geiger, S.; Zeradjanin, A. R.; Hodnik, N.; Kulyk, N.; Mayrhofer, K. J. J. Dissolution of Platinum in the Operational Range of Fuel Cells. *ChemElectroChem* **2015**, *2*, 1471–1478.
- (28) Topalov, A. A.; Cherevko, S.; Zeradjanin, A. R.; Meier, J. C.; Katsounaros, I.; Mayrhofer, K. J. J. Towards a Comprehensive Understanding of Platinum Dissolution in Acidic Media. *Chem. Sci.* **2014**, *5*, 631–638.
- (29) Borup, R.; Meyers, J.; Pivovar, B.; Kim, Y. S.; Mukundan, R.; Garland, N.; Myers, D.; Wilson, M.; Garzon, F.; Wood, D.; et al. Scientific Aspects of Polymer Electrolyte Fuel Cell Durability and Degradation. *Chem. Rev.* **2007**, *107*, 3904–3951.
- (30) Jung, W. S. Study on Durability of Pt Supported on Graphitized Carbon under Simulated Start-up/Shut-down Conditions for Polymer Electrolyte Membrane Fuel Cells. *J. Energy Chem.* **2018**, *27*, 326–334.
- (31) Jovanović, P.; Pavlišić, A.; Šelih, V. S.; Šala, M.; Hodnik, N.; Bele, M.; Hočevar, S.; Gabersček, M. New Insight into Platinum Dissolution from Nanoparticulate Platinum-Based Electrocatalysts Using Highly Sensitive in Situ Concentration Measurements. *ChemCatChem* **2014**, *6*, 449–453.
- (32) Gatalo, M.; Jovanović, P.; Polymeros, G.; Grote, J. P.; Pavlišić, A.; Ruiz-Zepeda, F.; Šelih, V. S.; Šala, M.; Hočevar, S.; Bele, M.; et al. Positive Effect of Surface Doping with Au on the Stability of Pt-Based Electrocatalysts. *ACS Catal.* **2016**, *6*, 1630–1634.
- (33) Jung, S. M.; Yun, S. W.; Kim, J. H.; You, S. H.; Park, J.; Lee, S.; Chang, S. H.; Chae, S. C.; Joo, S. H.; Jung, Y.; et al. Selective Electrocatalysis Imparted by Metal–Insulator Transition for Durability Enhancement of Automotive Fuel Cells. *Nat. Catal.* **2020**, *3*, 639–648.
- (34) Hodnik, N.; Zorko, M.; Jozinović, B.; Bele, M.; Dražić, G.; Hočevar, S.; Gabersček, M. Severe Accelerated Degradation of PEMFC Platinum Catalyst: A Thin Film IL-SEM Study. *Electrochem. Commun.* **2013**, *30*, 75–78.
- (35) Pavlišić, A.; Jovanović, P.; Šelih, V. S.; Šala, M.; Hodnik, N.; Hočevar, S.; Gabersček, M. The Influence of Chloride Impurities on Pt/C Fuel Cell Catalyst Corrosion. *Chem. Commun.* **2014**, *50*, 3732–3734.
- (36) Maselj, N.; Gatalo, M.; Ruiz-Zepeda, F.; Kregar, A.; Jovanović, P.; Hodnik, N.; Gabersček, M. The Importance of Temperature and Potential Window in Stability Evaluation of Supported Pt-Based Oxygen Reduction Reaction Electrocatalysts in Thin Film Rotating Disc Electrode Setup. *J. Electrochem. Soc.* **2020**, *167*, 114506.
- (37) Smiljanić, M.; Petek, U.; Bele, M.; Ruiz-Zepeda, F.; Šala, M.; Jovanović, P.; Gabersček, M.; Hodnik, N. Electrochemical Stability and Degradation Mechanisms of Commercial Carbon-Supported Gold Nanoparticles in Acidic Media. *J. Phys. Chem. C* **2021**, *125*, 635–647.
- (38) Jovanović, P.; Može, M.; Gričar, E.; Šala, M.; Ruiz-Zepeda, F.; Bele, M.; Marolt, G.; Hodnik, N. Effect of Particle Size on the Corrosion Behaviour of Gold in the Presence of Chloride Impurities: An EFC-ICP-MS Potentiodynamic Study. *Coatings* **2019**, *9* (1), 10.
- (39) Moriau, L. J.; Bele, M.; Vižintin, A.; Ruiz-Zepeda, F.; Petek, U.; Jovanović, P.; Šala, M.; Gabersček, M.; Hodnik, N. Synthesis and Advanced Electrochemical Characterization of Multifunctional Electrocatalytic Composite for Unitized Regenerative Fuel Cell. *ACS Catal.* **2019**, *9*, 11468–11483.
- (40) Hodnik, N.; Zorko, M.; Bele, M.; Hočevar, S.; Gabersček, M. Identical Location Scanning Electron Microscopy: A Case Study of Electrochemical Degradation of PtNi Nanoparticles Using a New Nondestructive Method. *J. Phys. Chem. C* **2012**, *116*, 21326–21333.
- (41) Hodnik, N.; Jovanović, P.; Pavlišić, A.; Jozinović, B.; Zorko, M.; Bele, M.; Šelih, V. S.; Šala, M.; Hočevar, S.; Gabersček, M. New Insights into Corrosion of Ruthenium and Ruthenium Oxide Nanoparticles in Acidic Media. *J. Phys. Chem. C* **2015**, *119*, 10140–10147.
- (42) Zalineeva, A.; Baranton, S.; Coutanceau, C.; Jerkiewicz, G. Electrochemical Behavior of Unsupported Shaped Palladium Nanoparticles. *Langmuir* **2015**, *31*, 1605–1609.
- (43) Bastide, S.; Zlotea, C.; Laurent, M.; Latroche, M.; Cachet-Vivier, C. Direct Assessment from Cyclic Voltammetry of Size Effect on the Hydrogen Sorption Properties of Pd Nanoparticle/Carbon Hybrids. *J. Electroanal. Chem.* **2013**, *706*, 33–39.
- (44) Łukaszewski, M.; Soszko, M.; Czerwiński, A. Electrochemical Methods of Real Surface Area Determination of Noble Metal Electrodes - an Overview. *Int. J. Electrochem. Sci.* **2016**, *11*, 4442–4469.
- (45) Meier, J. C.; Galeano, C.; Katsounaros, I.; Topalov, A. A.; Kostka, A.; Schüth, F.; Mayrhofer, K. J. J. Degradation Mechanisms of Pt/C Fuel Cell Catalysts under Simulated Start-Stop Conditions. *ACS Catal.* **2012**, *2*, 832–843.
- (46) Shao-Horn, Y.; Sheng, W. C.; Chen, S.; Ferreira, P. J.; Holby, E. F.; Morgan, D. Instability of Supported Platinum Nanoparticles in Low-Temperature Fuel Cells. *Top. Catal.* **2007**, *46*, 285–305.
- (47) Holby, E. F.; Sheng, W.; Shao-Horn, Y.; Morgan, D. Pt Nanoparticle Stability in PEM Fuel Cells: Influence of Particle Size Distribution and Crossover Hydrogen. *Energy Environ. Sci.* **2009**, *2*, 865–871.
- (48) Zhang, J.; Sasaki, K.; Sutter, E.; Adzic, R. R. Stabilization of Platinum. *Science* **2007**, *315*, 220–222.
- (49) <http://www.platinum.matthey.com/prices/price-charts> (accessed September 2021).



**JACS Au**  
AN OPEN ACCESS JOURNAL OF THE AMERICAN CHEMICAL SOCIETY

 Editor-in-Chief  
**Prof. Christopher W. Jones**  
Georgia Institute of Technology, USA

**Open for Submissions** 

[pubs.acs.org/jacsau](https://pubs.acs.org/jacsau)  **ACS Publications**  
Most-Used. Most Cited. Most Read.